



HAL
open science

Design and Fabrication of a Ring-Coupled Mach-Zehnder Interferometer Gyroscope

Eva Kempf, Pierre Labeye, Philippe Grosse, Frederic Boeuf, Stephane
Monfray, Paul Charette, Regis Orobtcouk

► **To cite this version:**

Eva Kempf, Pierre Labeye, Philippe Grosse, Frederic Boeuf, Stephane Monfray, et al.. Design and Fabrication of a Ring-Coupled Mach-Zehnder Interferometer Gyroscope. ESSCIRC 2021 - IEEE 47th European Solid State Circuits Conference (ESSCIRC), Sep 2021, Grenoble, France. pp.179-182, 10.1109/ESSCIRC53450.2021.9567877 . halshs-03515494

HAL Id: halshs-03515494

<https://shs.hal.science/halshs-03515494>

Submitted on 6 Jan 2022

HAL is a multi-disciplinary open access archive for the deposit and dissemination of scientific research documents, whether they are published or not. The documents may come from teaching and research institutions in France or abroad, or from public or private research centers.

L'archive ouverte pluridisciplinaire **HAL**, est destinée au dépôt et à la diffusion de documents scientifiques de niveau recherche, publiés ou non, émanant des établissements d'enseignement et de recherche français ou étrangers, des laboratoires publics ou privés.

Design and Fabrication of a Ring-Coupled Mach-Zehnder Interferometer Gyroscope

Eva Kempf
STMicroelectronics
Crolles, France
eva.kempf@st.com

Pierre Labeye
Département Optique et
Photonique (DOPT)
Commissariat à l'Énergie
Atomique et aux énergies
alternatives (CEA)
Grenoble, France
pierre.labeye@cea.fr

Philippe Grosse
Département Optique et
Photonique (DOPT)
Commissariat à l'Énergie
Atomique et aux énergies
alternatives (CEA)
Grenoble, France
philippe.grosse@cea.fr

Frédéric Boeuf
STMicroelectronics
Crolles, France
frederic.boeuf@st.com

Stéphane Monfray
STMicroelectronics
Crolles, France
stephane.monfray@st.com

Paul G. Charette
Laboratoire Nanotechnologies
Nanosystèmes (LN2 – IRL 3463)
Université de Sherbrooke - Institut
Interdisciplinaire d'Innovation
Technologique (3IT)
Sherbrooke, Canada
paul.charette@usherbrooke.ca

Régis Orobitchouk
Institut des Nanotechnologies de Lyon
(INL)
Institut des Sciences Nationales
Appliquées de Lyon (INSA)
Lyon, France
regis.orobitchouk@insa-lyon.fr

Abstract— In this paper, we present a CMOS-compatible integrated photonics resonant gyroscope incorporating active Si&Ge components with low-loss SiN waveguiding structures for the first time. The gyroscope design is based on a ring-coupled Mach-Zehnder interferometer (19.2 mm ring length). Based on numerical modelling, the estimated resolution is 1.08 deg/s, representing a 1.56-times improvement over a single ring all-pass design with the same footprint. Further improvement afforded by the MZI-based design is expected under Kerr effect limited conditions. Devices were fabricated with the STMicroelectronics DAPHNE (Datacom Advanced Photonics Nanoscale Environment) 300 mm Photonic R&D platform. Experimental measurements under static (non-rotating) conditions confirm the numerical modelling results.

Keywords— Integrated gyroscope, resonant gyroscope, SiN waveguide, Mach-Zehnder Interferometer

I. INTRODUCTION

Optical gyroscopes are angular velocity sensors based on the Sagnac effect [1], which causes a phase shift proportional to angular speed between two optical signals counter-propagating in a rotating loop. They have been used for decades in various domains, such as aeronautics, aerospace or military applications [2]. The most accurate gyroscopes are interferometric fiber optic gyroscopes (IFOG) and gyrolasers, which can reach inertial to tactical grade resolutions [3,4]. However, these gyroscopes are expensive and bulky, which makes them incompatible with mass-market production. More recently, emerging applications such as automotive, robotics, biomedical or consumer electronics have increased the demand for small footprints and low-cost gyroscopes [2,5]. Although micro-electro-mechanical systems (MEMS) offer a compact

alternative for cars and consumer electronics, they require vacuum packaging for high sensitivity [5] and cannot support high vibrations or accelerations [6].

Resonant fiber optic gyroscopes (RFOG), as their name implies, are based on fiber ring resonators and have twice the theoretical sensitivity of IFOGs for an equivalent footprint [7]. Indeed, shorter fiber lengths in RFOGs [5] without crossings result in lower losses [8]. RFOGs require a high coherence laser source, however, unlike IFOGs [1]. RFOG-type designs can be fabricated using integrated photonics, a leading technology for producing small footprint low-cost devices. Resonant gyroscope sensitivity, set by the slope of the response at resonance [9], is generally limited in high-performance devices by the Kerr effect, resulting from a power imbalance between the counter-propagating beams [10]. In 2009, Terrel *et al.* showed that coupling to a ring resonator via a Mach-Zehnder interferometer (MZI), termed a “Ring-coupled Mach-Zehnder interferometer” gyroscope, could improve the sensitivity of resonator-based gyroscopes as well as decrease the impact of the Kerr effect [11].

In this paper, we present the design and characterization of a novel SiN ring-coupled Mach-Zehnder interferometer gyroscope incorporating active Si & Ge components for the first time. The design shows a 1.56× improvement compared to state-of-the-art single-ring resonator integrated devices. The MZI-based design also leads to a decrease in noise due to the Kerr effect. The devices were fabricated on the STMicroelectronics 300 mm DAPHNE integrated photonics platform.

II. RING-COUPLED MZI GYROSCOPE : PROPOSED DESIGN

A. Description of the Fabricated Device

The devices were fabricated on the STMicroelectronics 300 mm DAPHNE industrial platform, which is capable of

co-integrating Si and SiN waveguides, active PN and PIN Si modulators, and Ge Photodiodes. A schematic of the design is given in Fig. 1. Light at $\lambda_0 = 1.31 \mu\text{m}$ (P_{in}) is injected into the input Si waveguide via a grating coupler and directed to the CCW(left)/CW(right) branches of the device with a 3dB coupler. Modulators (PIN/PN) in both branches are included for power balancing and modulation in future experiments. The signals are then split by Si-to-SiN tapers between the input power balance monitoring and normalization photodiodes (PDA, PDB) and the gyroscope SiN components (MZI and ring resonator). The upper (reference) arm of the MZI incorporates a heater that maintains a $\pm\pi/2$ phase shift to maximize sensitivity [11]. The lower arm of the MZI is coupled to the square-shaped ring resonator (4.8 mm on a side).

Fig. 2 shows a picture of the device after SiN layer deposition for the fabrication of the SiN waveguides. The corner sections are $600 \times 700 \text{ nm}$ cross-section single-mode waveguides (propagation losses: $\sim 0.5 \text{ dB/cm}$ [12]). The straight sections are multimode waveguides designed to minimize losses from sidewall roughness ($\sim 0.4 \text{ dB/cm}$, width = $1.3 \mu\text{m}$). The coupler between the lower arm of the MZI and the ring resonator was designed for critical

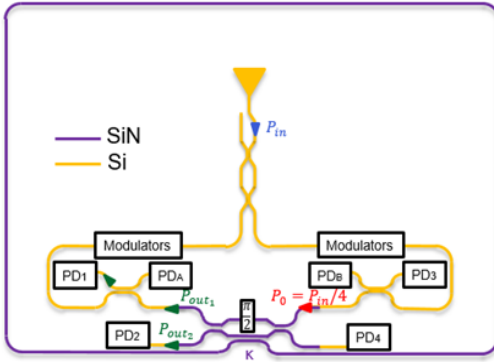


Fig. 1. Schematic of the ring-coupled Mach-Zehnder interferometer gyroscope. The PD1/PD2 and PD3/PD4 photodiode pairs enable quadrature measurements of the two counterpropagating optical signals in the ring, while photodiodes PDA and PDB are used for input power balance monitoring and normalization between the CW & CCW signals.

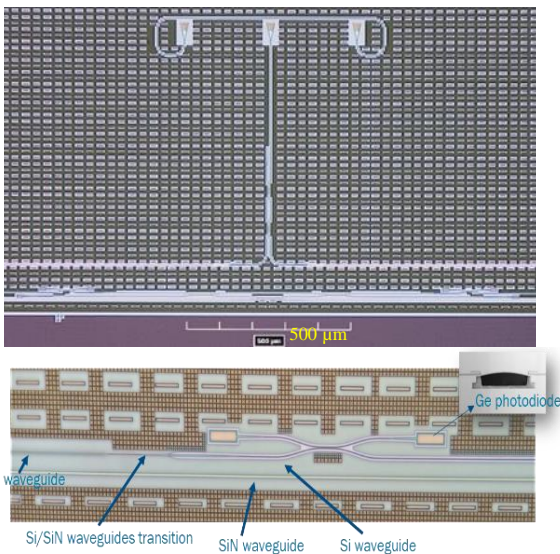


Fig. 2. TOP: Optical microscope picture of the gyroscope before deposition of the metal layers. BOTTOM: Si-to-SiN transition sections and Ge photodiodes.

coupling ($\kappa^2=15\%$). After counter-propagation in the ring, the two optical signals are routed to separate pairs of photodiodes (PD1/PD2, PD3/PD4) for differential measurements (see P_{out1} and P_{out2} in Fig.1 for the CW propagating path).

B. Mathematical Response

According to [15], the normalized photocurrents measured by the photodiode pairs from the two counter-propagating signals in a static gyroscope are given by:

$$\frac{PD_2}{PD_B} = \frac{PD_4}{PD_A} = \frac{1}{4} \cdot \left| \frac{\tau \cdot e^{-\frac{i2\pi nL}{\lambda} \cdot \frac{\alpha L}{2}} \cdot e^{-\frac{\alpha L}{2}}}{1 - \tau \cdot e^{-\frac{i2\pi nL}{\lambda} \cdot \frac{\alpha L}{2}}} + \sqrt{A} \cdot e^{i\pi\phi_s} \right|^2 \quad (1)$$

$$\frac{PD_1}{PD_B} = \frac{PD_3}{PD_A} = \frac{1}{2} \cdot \frac{1}{4} \cdot \left| -\frac{\tau \cdot e^{-\frac{i2\pi nL}{\lambda} \cdot \frac{\alpha L}{2}} \cdot e^{-\frac{\alpha L}{2}}}{1 - \tau \cdot e^{-\frac{i2\pi nL}{\lambda} \cdot \frac{\alpha L}{2}}} + \sqrt{A} \cdot e^{i\pi\phi_s} \right|^2 \quad (2)$$

where τ is the ring round-trip transmission coefficient, α is the ring propagation loss coefficient, L is the ring round-trip length, ϕ_s is the MZI phase shift, A is a factor accounting for losses in the upper MZI arm, n is the effective index of the guided mode, and λ is the wavelength. The quadrature arrangement of the PD1/PD2 and PD3/PD4 photodiode pairs at the opposite outputs of the interferometer enables differential measurements of the two counter-propagating signals, PD2-PD1 and PD4-PD3, yielding increased sensitivity [11]. Gyroscope sensitivity is maximized by measuring the change between the normalized differential signals, $(PD_4-PD_3)/PD_A - (PD_2-PD_1)/PD_B$, as a function of rotation.

C. Device Parameters Estimation

Experimental data were obtained by monitoring the photocurrents from all photodiodes while sweeping the source wavelength in steps of 1 pm. Use of the heater was not required as ϕ_s was already close to $-\pi/2$. Fig. 3 shows an example normalized transmission spectrum $(PD_4-PD_3)/PD_A$ and the corresponding fit to (1) and (2), where the maximum slope is $2.6 \cdot 10^{11} \text{ m}^{-1}$. For the $(PD_2-PD_1)/PD_B$ spectrum (not shown), the slope was slightly lower ($2.1 \cdot 10^{11} \text{ m}^{-1}$) due to a lower contrast, which may be corrected by optimizing the design. The ring parameters, $\tau = 85 \pm 0.5\%$, $\alpha = 0.4 \pm 0.02 \text{ dB/cm}$, and $n_{eff} = 1.748 \pm 0.01$ (guided mode effective index) were estimated with a mode solver. Based on these parameters, (1) and (2) were multiplied by an amplitude variable P_0 bounded to $[0.5, 1.5]$, and fitted to the experimental data using non-linear least squares to estimate the remaining unknown parameters, $A = 3.5 \pm 0.5 \text{ dB}$ and $\phi_s = -0.4\pi \pm 0.05\pi$.

III. RESONANT GYROSCOPE: PERFORMANCE ESTIMATION

A. Working Principle of Resonant Gyroscope

To compare gyroscope architectures, it is necessary to compute both sensitivity and resolution. Optical gyroscopes are based on the Sagnac effect. In ring-resonator based designs (Fig. 4), the resonance peaks in the transmission

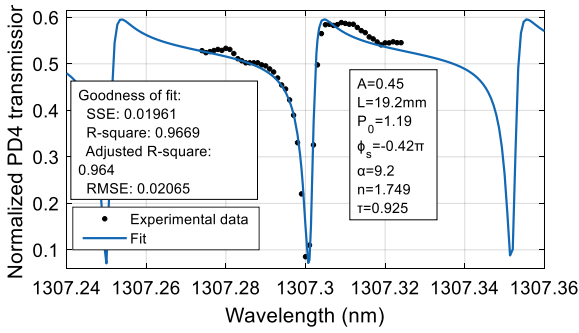


Fig. 3. Experimental data and corresponding fit to (1) and (2).

spectra for the counter-propagating optical signals incur equal and opposite shifts by $\Delta\nu$ [13]:

$$\Delta\nu = \frac{4A}{L \cdot n_{eff} \lambda_0} \cdot \Omega \quad (3)$$

where A is the ring area, L is its perimeter, n_{eff} is the guided mode effective index, λ_0 is the resonance wavelength in the absence of rotation, and Ω is the rotation speed.

In practice, one does not directly measure $\Delta\nu$, but rather the change in power output due to the shift at a fixed frequency ν_p [14] (Fig. 5). This frequency corresponds to the gyroscope operating point, where the slope in the transmission spectrum is at a maximum, and the response is considered quasi-linear over the operating range. A differential measurement from both counter-propagating signals maximizes the signal-to-noise ratio.

B. Resolution Estimation

The measurement resolution is defined as the change in rotation speed, $\delta\Omega$, corresponding to a signal level from the photodiodes that cannot be distinguished from the photocurrent standard deviation δi due to noise. Let $T(\nu_p, \Omega)$ be the ring resonator transmission at frequency ν_p and angular speed Ω . According to [9], the gyroscope resolution can be written as:

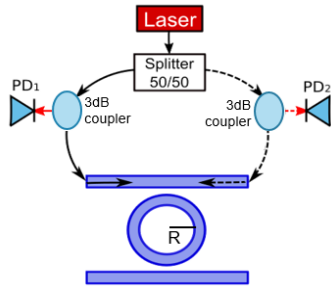


Fig. 4. Principle of resonant gyroscope.

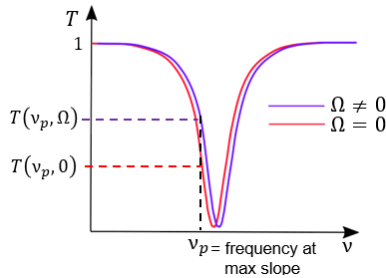


Fig. 5. Ring transmission T as a function of frequency with and without rotation

$$\delta\Omega = C \cdot \left(\frac{dT}{d\nu}(\nu_p) \right)^{-1} \cdot \frac{L \cdot n \cdot \lambda_0}{4A} \cdot \frac{\delta i}{i_D} \quad (4)$$

where $i_D = RP_{in}$ corresponds to the injected power, and C is a coefficient representing insertion losses. Sensitivity, S , defined as $S = C \cdot \left(\frac{dT}{d\nu}(\nu_p) \right)^{-1} \cdot \frac{Ln\lambda_0}{4A}$, is independent of the sources of noise and detection methods [14]. For a shot-noise limited system, δi is given by [9]:

$$\delta i = \sqrt{2qBR(P_{in} \cdot \max(T)/C)} \quad (5)$$

where q is the elementary charge, B is the bandwidth, R is the photodiode responsivity and $P_{in} \cdot \max(T)$ is the maximum power received by the photodiodes. From (4), one can see that the higher the slope of the resonance, the better the gyro resolution.

Coupling a ring resonator to a MZI with a $\pi/2$ phase shift in the reference arm yields sharp asymmetric Fano resonances [11,15]. In their article [11], M. Terrel *et al.* suggested that for low loss devices, the sharper slopes of Fano resonances compared to classical Lorentzian resonances could improve sensitivity by a factor of 1.305. In addition, they showed the interferometer-based design led to a 25% decrease in power circulating in the ring, which further reduced noise due to the Kerr effect.

Fig. 6-TOP shows modeled CW transmission spectra in the case of a static gyroscope for photodiode signals PD1 and PD2 and the differential result PD2-PD1 (normalized by $/PD_B$), assuming $A=1$ (no losses) and a MZI phase shift of $-\pi/2$ (all other ring parameters have estimated values stated above). Fig. 6-MID shows the modeled CW and CCW transmission spectra for cases of static and rotating gyroscopes (the 60k rads/s rotation rate is deliberately large for illustration purposes). Fig. 6-BOT shows the experimentally measured responses corresponding to Fig. 6-TOP, where the Fano resonance profiles are clearly visible. The shot noise limited resolution was computed using (4) and (5) with $C=4$ (signal power is divided by four before reaching the MZI), $\lambda = 1.31 \mu\text{m}$, $L = 19.2 \text{ mm}$, and $n_{eff} = 1.748$. The photodiode parameters were taken from [9]: responsivity $R = 0.72$, bandwidth $B = 10 \text{ Hz}$, and the injected power in the grating coupler was taken to be $P_{in} = 1 \text{ mW}$. Since two photodiodes are used in each direction for detection, their noise will add quadratically. We therefore need to compute the value $\max(T)$ for signals PD1+PD2 and PD3+PD4 and inject it in (5). For an all-pass ring resonator, the maximum value of transmission is determined by τ and is approximately equal to 1 when the losses are low. For this ring-coupled MZI, we computed the transmission maximum as $\max(\text{PD2}+\text{PD1}) \approx 0.79$.

Using the measured value of maximum slope from section II.C, we find an initial resolution estimate of $\delta\Omega = 2.13^\circ/\text{s}$. Note, however, that the frequency sampling resolution in Fig.3 was insufficient to fully resolve the resonance peaks, leading to an under-estimation of the maximum slope. Using the numerical model (Fig.6-MID) with $A = 1$ (assuming no losses in the MZI), $\phi_s = -\pi/2$, the maximum resonance slope $dT/d\nu$ was re-calculated, leading to a more realistic resolution estimate of $1.08^\circ/\text{s}$.

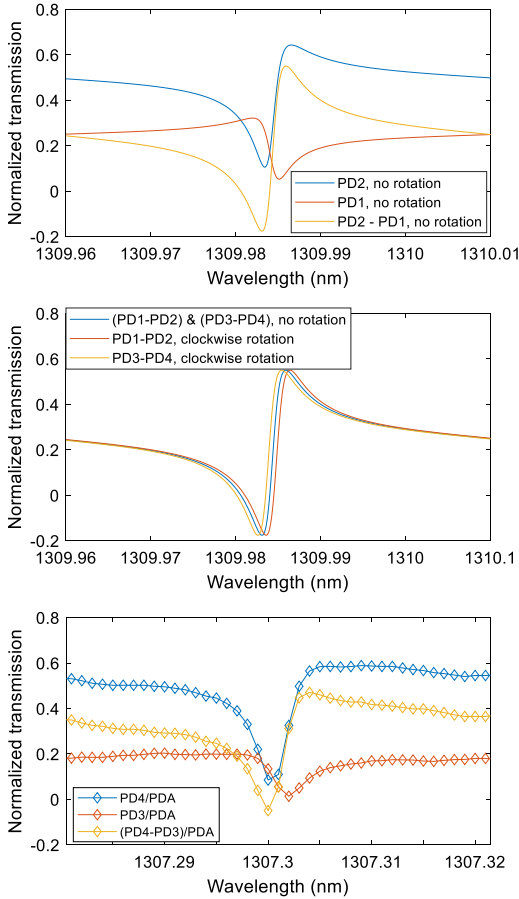


Fig.6. TOP: Modeled CW transmission spectra without rotation for photodiode outputs PD1 & PD2 and the differential signal PD2-PD1; MID: Modeled CW and CCW transmission spectra for the normalized differential signal pairs, PD1-PD2 and PD3-PD4, for static and rotating gyroscopes (60k rads/s CW); BOT: Experimental measurements corresponding to TOP.

C. Resolution Improvement Compared to a Single Ring All-pass Gyroscope

Compared to a single ring all-pass resonator without an interferometer with a similar footprint, the resonance slope, and thus the sensitivity, of the MZI-coupled design is multiplied by 1.305 [11]. To quantify the improvement in resolution, both the increase in slope and decrease in SNR must be taken into account. Considering the effect of the 3 dB couplers in both directions (25% power loss after circulating in the ring compared to 50% loss for an all-pass ring that would use two fewer photodiodes), the SNR is improved by a factor $0.75/0.5=1.5$. In addition, compared to a figure of 0.79 for the MZI-coupled gyro, the maximum transmission for an all-pass ring design would be around 0.5 because of the presence of a third 3 dB coupler before the detection photodiodes. This results in a combined SNR degradation of $\sqrt{0.79/0.5}=1.257$. As a result, the resolution improvement for the MZI-coupled design is $1.305 \cdot 1.5 / 1.257 = 1.56$. This improvement is even greater considering that the maximum injected power P_{max} is limited by the Kerr effect: since 25% less power is circulating in the ring for the MZI-coupled design compared to a single all-pass ring, we could inject 25% more power before being limited by the Kerr effect, and the total resolution improvement would therefore be $1.56 \cdot \sqrt{1.25} = 1.74$.

IV. CONCLUSION

A CMOS-compatible integrated SiN gyroscope based on a ring resonator coupled to a Mach-Zehnder interferometer manufactured on the STMicroelectronics 300 mm DAPHNE industrial platform was presented. A detailed characterization of the gyro performance was given, showing an estimated SNR improvement of 19.3% over a single ring all-pass design. Combined with the sensitivity gain from the sharp Fano resonances due to the MZI, the resolution at an input power of 1 mW was estimated at 2.13 $^{\circ}/s$. By refining the characterization measurements and optimizing the device, an estimated resolution of 1.08 $^{\circ}/s$ is expected. As a result, compared to a single ring all-pass with the same footprint, our design is expected to enhance the resolution by a factor $\times 1.56$. In addition, since 25% less power is circulating in the ring due to the MZI[12], this improvement could rise to $\times 1.74$ under conditions where the Kerr effect is the limiting noise factor. Experimental measurements under static conditions confirm the numerical modelling results.

V. ACKNOWLEDGMENTS

This work was supported by a European IPCEI program and IRT Nanoelec.

VI. REFERENCES

- [1] H. Lefèvre, *The fiber optic gyroscope : second edition*, 2014
- [2] F. Dell'io, T. Tatoli, C. Ciminelli, M. N. Armenise, "Recent advances in miniaturized optical gyroscopes", *J. Europ. Opt. Soc. Rap. Public.* 9,14013 (2014)
- [3] H. Lefèvre, " *Comprendre et apprécier le gyrofibre : le gyro aux performances ultimes ?* Photoniques 84, 40-43 (2016)
- [4] Alexia Ravaille, "Gyromètre optique basé sur une cavité résonante passive en fibre à cœur creux." *Optique [physics.optics]*. Université Paris-Saclay, 2018.
- [5] M. N. Armenis, C. Ciminelli, F. Dell'Olivo, V. M. N. Passaro, *Advances in gyroscope technologies* (2011)
- [6] V.Y. Venediktov, Y.V. Filatov, E.V. Shalymov, "Passive ring resonator micro-optical gyroscopes", *Quantum Electron.* 46 437 (2016)
- [7] M. Terrel, M.J.F Dignonnet, S. Fan, "Performance comparison of slow-light coupled-resonator optical gyroscopes", *Laser & Photon. Rev.* 3, No. 5, 452–465 (2009)
- [8] B. Wu, Y. Yu, J. Xiong, X. Zhang, "Silicon Integrated Interferometric Optical Gyroscope", *Scientific Reports*, 8:8766 (2018)
- [9] M.A. Guillén-Torres, E. Cretu, N.A.F. Jaeger, L. Chrostowski, "Ring Resonator Optical Gyroscopes—Parameter Optimization and Robustness Analysis", *J. Lightwave Technol.*, 0733-8724 (2012)
- [10] G. Feugnet, A. Ravaille, S. Schwartz, F. Bretenaker, "Analysis of the design of a passive resonant miniature optical gyroscope based on integrated optics technologies", *Optical Engineering*, 56(10), 107109 (2017).
- [11] M. Terrel, M.J.F Dignonnet, S. Fan, "Ring-coupled Mach-Zehnder interferometer optimized for sensing", *Applied Optics*, Vol. 48, Issue 26, pp. 4874-4879 (2009)
- [12] S. Guerber, "Intégration d'un deuxième niveau de guidage photonique par dépôt de SiN au-dessus du SOI traditionnel". *Optique / photonique*. Université Paris Saclay (COMUE), 2019.
- [13] G. B. Malykin, "Sagnac effect in ring lasers and ring resonators. How does the refractive index of the optical medium influence the sensitivity to rotation?" *Phys.-Usp.* 57 714 (2014)
- [14] M. Grant and M. Dignonnet. "Loss-gain coupled ring resonator gyroscope." *OPTO* (2019).
- [15] L. Zhou and A. W. Poon, "Fano resonance-based electrically reconfigurable add-drop filters in silicon microring resonator-coupled Mach-Zehnder interferometers", *Optics Letters* Vol. 32, Issue 7, pp 781-783 (2007).